Interaction Heterogeneity can Favorably Impact Colloidal Crystal Nucleation

Ian C. Jenkins, John C. Crocker, and Talid Sinno

Phys. Rev. Lett. **119**, 178002 — Published 23 October 2017

DOI: 10.1103/PhysRevLett.119.178002

The Surprising Role of Interaction Heterogeneity in Colloidal Crystallization

Ian C. Jenkins, John C. Crocker, and Talid Sinno[1]

Department of Chemical and Biomolecular Engineering,
University of Pennsylvania, Philadelphia, Pennsylvania 19104, USA

Abstract

Colloidal particles with short-ranged attractions, e.g., micron-scale spheres functionalized with single-stranded DNA oligomers, are susceptible to becoming trapped in disordered configurations even when a crystalline arrangement is the ground state. Moreover, for reasons that are not well understood, seemingly minor variations in the particle formulation can lead to dramatic changes in the crystallization outcome. We demonstrate, using a combination of equilibrium and non-equilibrium computer simulations, that interaction heterogeneity—variations in the energetic interactions among different particle pairs in the population—may favorably impact crystal nucleation. Specifically, interaction heterogeneity is found to lower the free energy barrier to nucleation via the formation of clusters comprised preferentially of strong-binding particle pairs. Moreover, gelation is inhibited by 'spreading out over time' the nucleation process, resulting in a reduced density of stable nuclei, allowing each to grow unhindered and larger. Our results suggest a simple and robust approach for enhancing colloidal crystallization near the 'sticky sphere' limit, and support the notion that differing extents of interaction heterogeneity arising from various particle functionalization protocols may contribute to the otherwise unexplained variations in crystallization outcomes reported in the literature.

PACS: 64.60.-i, 64.60.Q-, 64.70.-p, 64.75.Xc

Keywords: Crystallization, Aggregation, Clustering, Nucleation, Self-assembly

[1] Corresponding author: talid@seas.upenn.edu, Tel: (215) 898-2511

The use of short, synthetic DNA strands grafted onto the surfaces of particles to drive them to assemble into crystalline structures is being actively investigated as a paradigm for 'programmable' self-assembly [1-4]. DNA-mediated assembly has now been demonstrated widely in experiment with both nanoparticles [1, 5-7] and colloidal microspheres [8-14]. These efforts have been supported by accurate simulations [15-18], which have identified various thermodynamic [19-21] and kinetic [22-28] bottlenecks. The predictions of simulations notwithstanding, experimental progress, particularly for micron-scale colloidal crystallization, has been hampered by several factors. First, for reasons that are still not fully understood, some of the earlier chemical protocols used to graft DNA oligomers resulted in particles that formed disordered aggregates rather than crystals [29-31]. This was resolved with the introduction of the swelling/deswelling grafting technique for polystyrene particles [32] in 2005, leading to the first demonstrations of reversibly-bound colloidal crystals [8]; recently, grafting approaches have been successfully demonstrated for other types of particles [33]. Nonetheless, numerous constraints must be navigated carefully to obtain kinetically facile and high quality crystal growth. For example, while a particular binding energy between two microspheres may be achieved in a number of ways—by varying the DNA hybridization free energy, the temperature, and/or the DNA grafting density—in practice, good crystals only form for some combinations of these parameters. Generally, low grafting densities of DNA oligomers lead to slower binding kinetics [29, 34] and larger density fluctuations, or 'patchiness', on a particle's surface, possibly creating obstacles to annealing by particle rolling and sliding [35]. Perhaps most crucially, crystallization of micron-scale particles via short-ranged interactions is known to be inherently difficult, requiring a narrow range of inter-particle binding strengths—too weak and the nucleation rate of crystallites is slow or fails to occur altogether, too strong and the system can become trapped by system-wide gelation into a metastable, disordered state [13, 24, 36, 37]. This latter pathway to disorder is universal to systems with short-ranged interactions, and acts additionally to (and is distinct from) those arising from specific particle preparation peculiarities that may inhibit local relaxation

processes. For ensembles of DNA-functionalized particles, the width of the crystallization window may be especially narrow due to the multivalent nature of DNA-mediated attractions [16, 30, 38-41] and several approaches for engineering the window for DNA-mediated crystallization have been proposed, including temperature cycling [26], introducing mobile DNA strands on particle surfaces [42, 43], and alterations of the DNA bridge architecture to modify the phase behavior [10, 14, 39, 44].

Here, we propose a previously unexplored mechanism—interaction heterogeneity—for enhancing the crystallization window, which may also contribute to the currently unexplained variability in experimental observations of crystallization of DNA-grafted microspheres (and other types of sticky-sphere colloids). In the context of DNA-functionalized particles, the heterogeneity described in the present paper refers to variability in the grafted DNA oligonucleotide density *across the particle population*, and is distinct from *single-particle* heterogeneity in the spatial distribution of strands on one particle. We show that this type of heterogeneity, which produces a distribution of interaction strengths among pairs of particles, leads to increased crystallization robustness by (1) lowering the mean binding energy needed for crystallization, and (2) widening the crystallization window. This is unexpected given that heterogeneity is conventionally regarded as being detrimental to crystallization [45]. Unfortunately, quantitative experimental measurements of DNA-mediated interaction heterogeneity are scarce: Casey [46] has reported that one DNA-colloid formulation approach that led to crystallization also possessed a wide dispersion in the DNA density (standard deviation ~15%) among individual particles, while Dreyfus et al. [47] estimated an interaction heterogeneity <10%, although no corresponding crystallization studies were performed.

We consider a single-component system of 1 micron-diameter spherical particles that interact via a validated coarse-grained pair potential function [16]. Inter-particle interaction heterogeneity was modeled by randomly assigning each particle, i, a binding multiplier, b_i, where the value of b_i is generated from a Gaussian distribution with unit mean and standard deviation p. The binding multiplier

thus encodes the DNA density on a given particle and the interaction potential energy between two particles, *i* and *j*, is given by

$$U_{ij}(r) = b_i b_j U_{DNA}(r), \tag{1}$$

where $U_{DNA}(r)$ represents the mean DNA potential energy as a function of inter-particle separation.

Nucleation free energy profiles for crystallites were computed using umbrella sampling Metropolis Monte Carlo (MMC) simulations [48]. These simulations were initiated by placing a spherical random hexagonally close-packed (rhcp) crystallite (the ground state configuration) of a desired size in an equilibrated colloidal fluid (2000 particles at volume fraction 10%). All particles were assigned *b* values drawn randomly from the Gaussian binding distribution. A bias potential of the form

$$U_B = \frac{k}{2}(n - n_T)^2, \tag{2}$$

was added to the interaction potential, where n is the size of the rhcp crystallite computed according to Ref. [49], n_T is the target crystallite size, and k (0.125 $k_B T$ for all simulations) is the bias strength. Umbrella sampling simulations were executed by generating sequences of 1000 MMC sweeps over all particles using the usual Metropolis criterion to accept or reject each particle displacement attempt [50]. Binding factor exchanges between random pairs of particles also were attempted, on average, once every sweep over displacement moves. Each 1000-sweep sequence was then accepted or rejected with an additional Metropolis test based on the change in the bias potential, ΔU_B. A simulation was terminated—typically after ~10^6 sweeps—once the average crystallite size, $\langle n \rangle_B$, was converged to less than 1% variation over sequential, non-overlapping intervals of 10^5 sweeps.

Direct non-equilibrium simulations of crystallite nucleation and growth also were carried out with NVT-ensemble MMC; MMC was employed to simplify the implementation of heterogeneous interactions

between particles. In each of these simulations, a periodic system of 2000 particles at a volume fraction of 10% was first equilibrated in the fluid phase by artificially lowering the interaction strength. The interaction strength and heterogeneity were then increased to the desired levels and the system allowed to evolve until crystallization was observed, or the simulation terminated. Direct growth simulations were performed only using small displacement moves (max. move size ~ 0.04 μm corresponding to a target move acceptance probability of 40-50%), i.e., bias-free and without binding factor exchanges. The appropriate use of small-displacement move MMC for non-equilibrium simulations has been discussed in detail in previous work [22, 51], where the equivalence of BD and MMC for generating overdamped Langevin dynamics trajectories has been demonstrated. A series of control simulations for a homogeneous interaction system were performed to ensure (1) that changing the acceptance criterion (and therefore the maximum particle displacement) did not alter the evolution of the cluster distribution, and (2) that the MMC results were in quantitative agreement with reference Brownian dynamics simulations.

The equilibrium nucleation free energy barriers, $\Delta G_{\max}$, for several average binding energies, $3.0 \le \langle \beta U \rangle \le 4.0$, as a function of interaction heterogeneity, p, are shown in Fig. 1. The quantity $\langle \beta U \rangle$ here refers to the average value of the maximum attractive energy (scaled by $k_B T$), or 'potential well-depth', between a pair of particles. The free energy barriers represent peaks of the nucleation free energy curves across a range of crystallite sizes—see inset of Fig. 1. The impact of interaction heterogeneity on the nucleation barrier is profound, particularly for weak average binding. For $\langle \beta U \rangle = 3.2$ (blue), the addition of just 10% heterogeneity (p = 0.10) reduces the barrier from 75 $k_B T$ to ~15 $k_B T$. For a slightly weaker binding energy, $\langle \beta U \rangle = 3.0$, the barrier for the heterogeneity-free system is effectively infinite because the fluid phase is the ground state—again, for p = 0.10, the barrier drops to ~20 $k_B T$. For typical diffusion coefficients exhibited by micron-scale particles in water (~0.5 μm^2/s), these results imply that a

uniform system with $3.0 \le \langle \beta U \rangle \le 3.2$ would not be expected to exhibit any crystallization, while the heterogeneous ones would crystallize rapidly in minutes to hours.

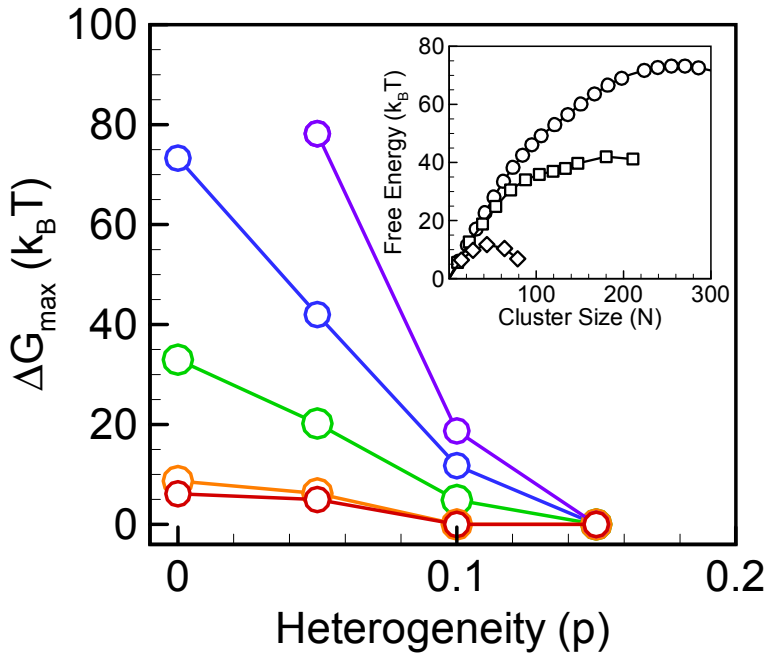

Figure 1: Interaction heterogeneity reduces nucleation barrier height and critical nucleus size: purple – $\langle \beta U \rangle = 3.0$, blue – $\langle \beta U \rangle = 3.2$, green – $\langle \beta U \rangle = 3.4$, orange – $\langle \beta U \rangle = 3.8$, red – $\langle \beta U \rangle = 4.0$. Inset: free energy profiles as a function of cluster size for $\langle \beta U \rangle = 3.2$: circles – p = 0, squares – p = 0.05, diamonds – p = 0.10.

The impact of heterogeneity may be understood qualitatively by particle fractionation: the subset of the most strongly interacting particles reduce the overall nucleation barrier by assembling into nuclei that are more stable than ones formed from 'average' particles. Shown in Fig. 2(a) are spherically-averaged distributions of normalized binding energies, for three different combinations of average binding energy and heterogeneity, as a function of distance from the center-of-mass of equilibrium

clusters. Corresponding configuration snapshots are shown in Figs. 2(b-d). In each case, crystallites exhibit a core region of particles with strongly enhanced binding (approx. 1.5-2 standard deviations above the mean binding energy) and a transition region corresponding to the outermost one or two particle shells across which the average binding strength decreases gradually towards the background fluid value.

While mechanistically informative, equilibrium calculations do not properly reflect experimental conditions, which are intrinsically non-equilibrium. Most importantly, the finite growth rate of a crystallite places a limitation on the length scale over which the crystallite can sample and recruit particles by diffusion. By contrast, equilibrium conditions assume that a growing crystal nucleus may incorporate particles from anywhere in the entire domain, no matter how large it may be—resulting in an artificial finite system size effect. These differences may be understood more quantitatively by considering a growth timescale, τ_g, for adding a monolayer of particles to a growing crystallite, and a diffusion timescale, $\tau_d = L_d^2 / D$, where L_d is the capture radius for particles. The maximum capture radius is then given by the condition $\tau_d \sim \tau_g$, or $L_d \sim \left(D\tau_g \right)^{1/2}$. Thus, for finite crystallite growth rate, L_d is the length scale beyond which system size becomes irrelevant. The further away from equilibrium the system is driven, the faster crystallite growth becomes and the smaller the capture radius, reducing the impact of heterogeneity.

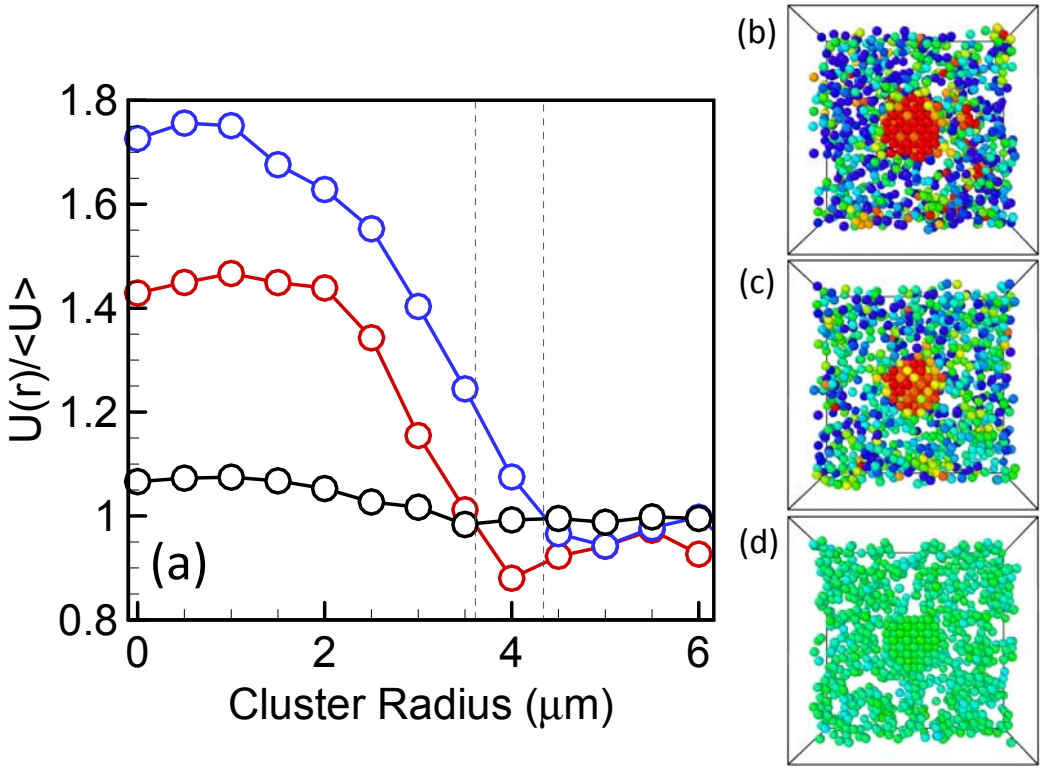

Figure 2: (a) Radial fractionation of particle binding strengths in crystallites: blue – $\langle \beta U \rangle = 3.0$, p = 0.39, red – $\langle \beta U \rangle = 3.4$, p = 0.25, and black – $\langle \beta U \rangle = 5.5$, p = 0.05. The vertical dashed lines approximately denote the cluster-fluid interface location. (b-d) Snapshots of mid-plane slices through the corresponding simulation domains (in order of decreasing heterogeneity) showing enhanced binders in the crystallites located at the center. Green color is the mean value (b = 1), red is highest (b = 1.5), blue is lowest (b = 0.67).

The impact of finite growth rate is demonstrated in Fig. 3, which shows the radial distribution of normalized binding energies in clusters that were spontaneously nucleated at the same three conditions in Fig. 2. As expected, the non-equilibrium fractionation effect is substantially weaker than the corresponding equilibrium situation because of capture zone limitations. At low average binding energy (corresponding to low growth rate) and high heterogeneity (blue, $\langle \beta U \rangle = 3.0$, p = 0.39), the maximum

binding energy enhancement, about one standard deviation above the mean or 40%, is located immediately at the center of crystallites and rapidly decreases away from the center to about 10%. Similar behavior is observed for the medium binding energy and heterogeneity case (red, $\langle \beta U \rangle = 3.4$, $p = 0.25$). For high binding energy and low heterogeneity (black, $\langle \beta U \rangle = 5.4$, $p = 0.05$), essentially no binding enhancement is observed—crystallites grow so rapidly that they incorporate whatever particles are nearby. The insets in Fig. 3 show examples of mid-plane slices through corresponding crystallites.

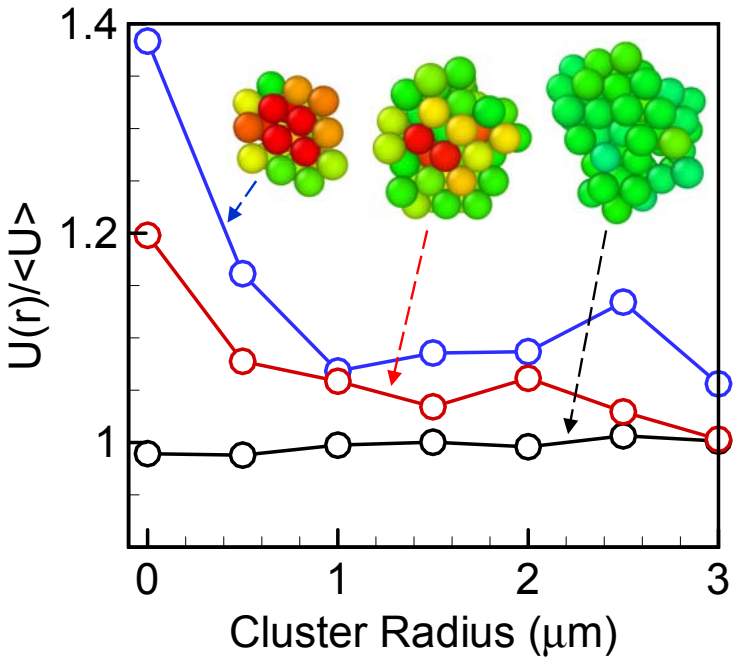

Figure 3: Radial fractionation of binding strengths in clusters nucleated and grown spontaneously under non-equilibrium conditions: blue – $\langle \beta U \rangle = 3.0$, $p = 0.39$, red – $\langle \beta U \rangle = 3.4$, $p = 0.25$, and black – $\langle \beta U \rangle = 5.5$, $p = 0.05$. Insets: mid-plane slices through crystallites showing binding strength distribution; green color is the mean value ($b = 1$), red is highest ($b = 1.5$), blue is lowest ($b = 0.67$).

The preceding results indicate that nucleation rates of colloidal crystals are generally accelerated by interaction heterogeneity, to an extent that depends on how fast crystallites are growing relative to particle diffusion. While interesting, this effect is not obviously of practical relevance to colloidal crystallization—the nucleation rate may be readily controlled by the average binding energy in a homogeneous system. But additional analysis reveals that interaction heterogeneity also plays a more subtle role—it inhibits the system-wide gelation process described by Lu et al. [37]. To assess the impact of heterogeneity on gelation, a large number of direct, non-equilibrium crystallization simulations at various combinations of interaction heterogeneity and average binding strength were performed. Samples of particle configurations after about 10^6 MMC sweeps (after which the system evolution slows dramatically) are shown in Fig. 4. The top row exhibits configurations that result without interaction heterogeneity across a binding energy interval, $4.8 \le \langle \beta U \rangle \le 5.8$, in which the system transitions sensitively from exhibiting no nucleation, to showing a few isolated, highly crystalline clusters, to gelation in which a connected network of elongated, disorganized clusters is formed across the entire domain, reminiscent of the gelled states observed by Lu et al. [37]. The remarkable impact of heterogeneity is demonstrated in the bottom row, which shows configurations with p = 0.15 over an equally wide average binding energy interval, $3.6 \le \langle \beta U \rangle \le 4.6$. Here, the relevant binding energy is shifted to lower mean values, and much more significantly, the configurations now reflect a gradual increase in the nucleation rate, exhibiting largely isolated crystallites across the binding energy interval.

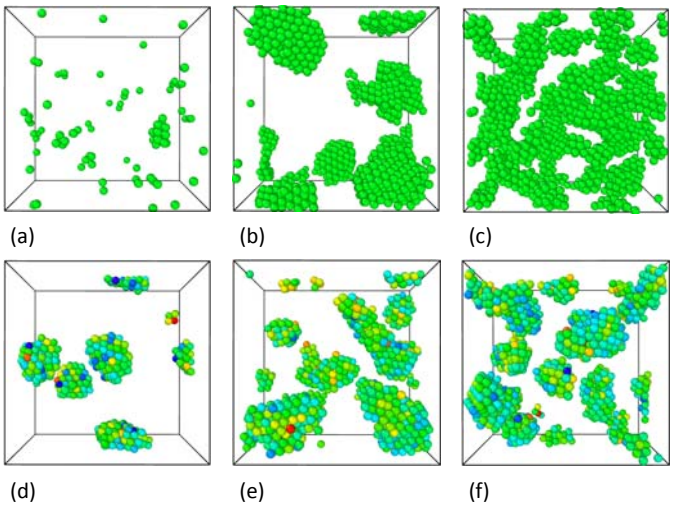

Figure 4: Interaction heterogeneity widens the crystallization window. Final configurations (see text) as a function of interaction strength for p = 0 [top row, $\langle \beta U \rangle =$ 4.8 (a), 5.2 (b), and 5.8 (c)] and p = 0.15 [bottom row, $\langle \beta U \rangle =$ 3.6 (d), 4.0 (e), and 4.6 (f)]. Particle color represents binding strength: green is the mean value, red is higher, blue is lower.

These observations are summarized into a more comprehensive view in Fig. 5, which shows a field map of the maximum cluster number density (ϕ, clusters per cm^3) as a function of average binding strength and heterogeneity. The maximum crystallite number density is used here to distinguish between crystallization and gelation outcomes. The blue region (lower left, $\phi < 2\times10^8$ cm^{-3}) corresponds to no crystallites being observed over the length of our simulations, while the white region (upper right, $\phi > 2.5\times10^9$ cm^{-3}) generally corresponds to gelation outcomes with large numbers of aggregates forming a connected and arrested network. In between these limits exists a bounded region (between the dashed lines) that, roughly speaking, is the crystallization window, which is clearly widened by heterogeneity. The 6 configuration snapshots shown previously in Fig. 4 at p = 0 and p = 0.15 are each denoted by a circle in Fig. 5—all 3 lie in the crystallization window for p = 0.15, while only a single state

point does at $p = 0$. Moreover, since the strength of DNA interactions is typically an exponential function of temperature, the translation of the crystallization window to weaker interactions implies that the temperature window for crystallization exhibits an even greater widening effect than indicated here.

Our findings regarding the width of the crystallization window compare favorably to experimental results in the literature. Kim et al. [29] incubated in parallel matched samples of micron-sized colloids bearing ~4000 DNA strands per particle, at temperatures spaced out by 0.25 °C, and found that typically only one or two samples yielded crystals; suggesting a window width of ~0.4 °C. Direct interaction measurements on the same samples, reported by Biancaniello et al. [8], indicate that the attractive interaction increases roughly exponentially with falling temperature, by ~10% per 0.2 °C. Combining these results suggests that the crystallization window has a width of ~20-25% in interaction strength, which is comparable to the window prediction at $p = 0.15$ in Fig. 5, and much wider than the ~8% window width at $p = 0$. Moreover, measurements of similar samples formed by the same protocol, reported by Casey [46], found a heterogeneity of $p = 0.15$, providing additional experimental support for the results of our non-equilibrium crystallization simulations.

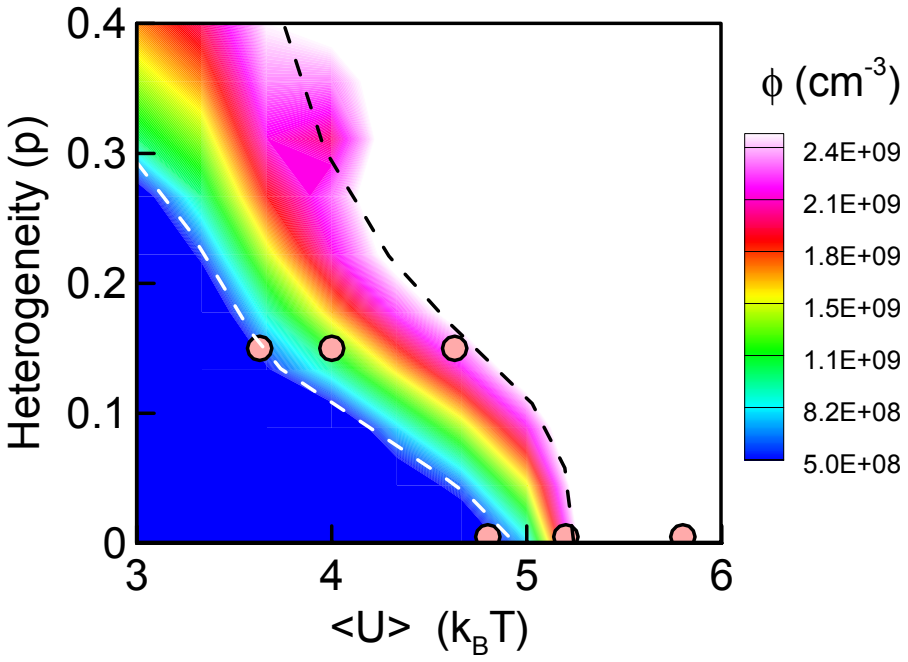

Figure 5: Interaction heterogeneity lowers and widens the window for crystallization. Color field denotes the maximum cluster number density, ϕ, as a function of average binding strength and heterogeneity. Thin lines represent isolines of nucleation barrier height, $\beta\Delta G_{\max}$, with values (upper left to lower right): 1, 2, 3, 5, 30, and 90 $k_B T$. Dashed lines schematically denote crystallization window. Diamond symbols show locations of corresponding to the configurations snapshots shown in Fig. 4.

The crystallization window opening effect may be attributed to the buffering action of heterogeneity—strong binders that locally drive nucleation of crystallites are dispersed among weaker binders that interfere with the onset of the system-wide spinodal decomposition associated with gelation that was described in Ref. [37]. In the context of a typical crystallization experiment with DNA-functionalized particles, where the temperature is gradually reduced to increase the thermodynamic driving force for condensation by increasing the DNA-mediated attractions between particles, heterogeneity acts to spread out nucleation into a gentler, sequential process in which progressively

weaker binders are able to form stable nuclei. This sequentialization of the nucleation process is akin to a 'controlled burn' rather than the typical explosive nucleation that is characteristic of strongly driven systems. Given the likely ubiquitous presence of at least some degree of particle-to-particle heterogeneity in engineered systems such as DNA-functionalized particle assemblies, this mechanism may in fact have been operative, but unappreciated, in many instances to date. Note that the present findings are agnostic with respect to the source of attractive inter-particle potentials and could be also be applicable to other aggregating systems, e.g., those driven by depletion [52-55]. It is less clear what would cause interaction heterogeneity in depletion systems but one possibility would be slight zeta-potential variations between different particles altering the excluded volume associated with charged depletant species. Perhaps most significantly, our results suggest a facile avenue for optimizing crystallization behavior in systems where the interactions may be purposefully tuned across a population of particles, such as the DNA-driven one we consider here.

Acknowledgements: We gratefully acknowledge financial support from the National Science Foundation under Awards CBET-0829045 and CBET-1133386. We also thank Amish Patel for useful discussions regarding the sparse umbrella sampling simulations.

References:

1. S. Y. Park, A. K. R. Lytton-Jean, B. Lee, S. Weigand, G. C. Schatz, and C. A. Mirkin, "DNA-programmable nanoparticle crystallization," Nature **451**, 553-556 (2008).
2. Y. Zhang, F. Lu, K. G. Yager, D. van der Lelie, and O. Gang, "A general strategy for the DNA-mediated self-assembly of functional nanoparticles into heterogeneous systems," Nat Nanotechnol **8**, 865-872 (2013).
3. W. B. Rogers, W. M. Shih, and V. N. Manoharan, "Using DNA to program the self-assembly of colloidal nanoparticles and microparticles," Nature Reviews Materials **1**, 16008 (2016).
4. Y. Zhang, S. Pal, B. Srinivasan, T. Vo, S. Kumar, and O. Gang, "Selective transformations between nanoparticle superlattices via the reprogramming of DNA-mediated interactions," Nat Mater **14**, 840-847 (2015).
5. D. Nykypanchuk, M. M. Maye, D. van der Lelie, and O. Gang, "DNA-guided crystallization of colloidal nanoparticles," Nature **451**, 549-552 (2008).

6. R. J. Macfarlane, B. Lee, M. R. Jones, N. Harris, G. C. Schatz, and C. A. Mirkin, "Nanoparticle Superlattice Engineering with DNA," Science **334**, 204-208 (2011).
7. E. Auyeung, T. I. Li, A. J. Senesi, A. L. Schmucker, B. C. Pals, M. O. de La Cruz, and C. A. Mirkin, "DNA-mediated nanoparticle crystallization into Wulff polyhedra," Nature **505**, 73-77 (2014).
8. P. L. Biancaniello, A. J. Kim, and J. C. Crocker, "Colloidal interactions and self-assembly using DNA hybridization," Phys Rev Lett **94**, - (2005).
9. A. J. Kim, R. Scarlett, P. L. Biancaniello, T. Sinno, and J. C. Crocker, "Probing interfacial equilibration in microsphere crystals formed by DNA-directed assembly," Nat Mater **8**, 52-55 (2009).
10. M. T. Casey, R. T. Scarlett, W. B. Rogers, I. Jenkins, T. Sinno, and J. C. Crocker, "Driving diffusionless transformations in colloidal crystals using DNA handshaking," Nat Commun **3**, (2012).
11. J. T. McGinley, I. Jenkins, T. Sinno, and J. C. Crocker, "Assembling colloidal clusters using crystalline templates and reprogrammable DNA interactions," Soft Matter **9**, 9119-91289119 (2013).
12. J. T. McGinley, Y. Wang, I. C. Jenkins, T. Sinno, and J. C. Crocker, "Crystal-Templated Colloidal Clusters Exhibit Directional DNA Interactions," Acs Nano **9**, 10817-10825 (2015).
13. Y. Wang, Y. Wang, X. Zheng, É. Ducrot, J. S. Yodh, M. Weck, and D. J. Pine, "Crystallization of DNA-coated colloids," Nat Commun **6**, (2015).
14. W. B. Rogers and V. N. Manoharan, "Programming colloidal phase transitions with DNA strand displacement," Science **347**, 639-642 (2015).
15. J. Largo, F. W. Starr, and F. Sciortino, "Self-Assemblong DNA Dendrimers: A Numerical Study," Langmuir **23**, 5896-5905 (2007).
16. W. B. Rogers and J. C. Crocker, "Direct measurements of DNA-mediated colloidal interactions and their quantitative modeling," P Natl Acad Sci USA **108**, 15687-15692 (2011).
17. M. E. Leunissen and D. Frenkel, "Numerical study of DNA-functionalized microparticles and nanoparticles: Explicit pair potentials and their implications for phase behavior," J Chem Phys **134**, (2011).
18. B. M. Mognetti, P. Varilly, S. Angioletti-Uberti, F. J. Martinez-Veracoechea, J. Dobnikar, M. E. Leunissen, and D. Frenkel, "Predicting DNA-mediated colloidal pair interactions," P Natl Acad Sci USA **109**, E378-E379 (2012).
19. F. V. Lara and F. W. Starr, "Stability of DNA-linked nanoparticle crystals I: Effect of linker sequence and length," Soft Matter **7**, 2085-2093 (2011).
20. O. Padovan-Merhar, F. V. Lara, and F. W. Starr, "Stability of DNA-linked nanoparticle crystals: Effect of number of strands, core size, and rigidity of strand attachment," J Chem Phys **134**, (2011).
21. T. I. Li, R. Sknepnek, R. J. Macfarlane, C. A. Mirkin, and M. Olvera de la Cruz, "Modeling the crystallization of spherical nucleic acid nanoparticle conjugates with molecular dynamics simulations," Nano letters **12**, 2509-2514 (2012).
22. R. T. Scarlett, J. C. Crocker, and T. Sinno, "Computational analysis of binary segregation during colloidal crystallization with DNA-mediated interactions," J Chem Phys **132**, (2010).
23. R. T. Scarlett, M. T. Ung, J. C. Crocker, and T. Sinno, "A mechanistic view of binary colloidal superlattice formation using DNA-directed interactions," Soft Matter **7**, 1912-1925 (2011).
24. L. Di Michele, F. Varrato, J. Kotar, S. H. Nathan, G. Foffi, and E. Eiser, "Multistep kinetic self-assembly of DNA-coated colloids," Nat Commun **4**, (2013).

25. I. C. Jenkins, M. T. Casey, J. T. McGinley, J. C. Crocker, and T. Sinno, "Hydrodynamics selects the pathway for displacive transformations in DNA-linked colloidal crystallites," Proceedings of the National Academy of Sciences **111**, 4803-4808 (2014).
26. C. Knorowski and A. Travesset, "Dynamics of DNA-programmable nanoparticle crystallization: gelation, nucleation and topological defects," Soft Matter **8**, 12053-12059 (2012).
27. W. Dai, S. K. Kumar, and F. W. Starr, "Universal two-step crystallization of DNA-functionalized nanoparticles," Soft Matter **6**, 6130-6135 (2010).
28. M. E. Leunissen, R. Dreyfus, R. Sha, N. C. Seeman, and P. M. Chaikin, "Quantitative Study of the Association Thermodynamics and Kinetics of DNA-Coated Particles for Different Functionalization Schemes," J Am Chem Soc **132**, 1903-1913 (2010).
29. A. J. Kim, P. L. Biancaniello, and J. C. Crocker, "Engineering DNA-mediated colloidal crystallization," Langmuir **22**, 1991-2001 (2006).
30. N. Geerts and E. Eiser, "DNA-functionalized colloids: Physical properties and applications," Soft Matter **6**, 4647-4660 (2010).
31. L. Di Michele and E. Eiser, "Developments in understanding and controlling self assembly of DNA-functionalized colloids," Phys Chem Chem Phys **15**, 3115-3129 (2013).
32. A. J. Kim, V. N. Manoharan, and J. C. Crocker, "Swelling-based method for preparing stable, functionalized polymer colloids," J Am Chem Soc **127**, 1592-1593 (2005).
33. Y. Wang, Y. Wang, X. Zheng, E. t. Ducrot, M.-G. Lee, G.-R. Yi, M. Weck, and D. J. Pine, "Synthetic strategies toward DNA-coated colloids that crystallize," J Am Chem Soc **137**, 10760-10766 (2015).
34. W. B. Rogers, T. Sinno, and J. C. Crocker, "Kinetics and non-exponential binding of DNA-coated colloids," Soft Matter **9**, 6412-6417 (2013).
35. Q. Xu, L. Feng, R. Sha, N. Seeman, and P. Chaikin, "Subdiffusion of a sticky particle on a surface," Phys Rev Lett **106**, 228102 (2011).
36. P. L. Biancaniello, J. C. Crocker, D. A. Hammer, and V. T. Milam, "DNA-mediated phase behavior of microsphere suspensions," Langmuir **23**, 2688-2693 (2007).
37. P. J. Lu, E. Zaccarelli, F. Ciulla, A. B. Schofield, F. Sciortino, and D. A. Weitz, "Gelation of particles with short-range attraction," Nature **453**, 499-504 (2008).
38. R. Dreyfus, M. E. Leunissen, R. Sha, A. Tkachenko, N. C. Seeman, D. J. Pine, and P. M. Chaikin, "Aggregation-disaggregation transition of DNA-coated colloids: Experiments and theory," Phys Rev E **81**, 041404 (2010).
39. B. M. Mognetti, M. E. Leunissen, and D. Frenkel, "Controlling the temperature sensitivity of DNA-mediated colloidal interactions through competing linkages," Soft Matter **8**, 2213-2221 (2012).
40. S. Angioletti-Uberti, B. M. Mognetti, and D. Frenkel, "Theory and simulation of DNA-coated colloids: a guide for rational design," Phys Chem Chem Phys **18**, 6373-6393 (2016).
41. S. J. Bachmann, M. Petitzon, and B. M. Mognetti, "Bond formation kinetics affects self-assembly directed by ligand–receptor interactions," Soft Matter **12**, 9585-9592 (2016).
42. S. A. van der Meulen and M. E. Leunissen, "Solid colloids with surface-mobile DNA linkers," J Am Chem Soc **135**, 15129-15134 (2013).
43. S. Angioletti-Uberti, P. Varilly, B. M. Mognetti, and D. Frenkel, "Mobile linkers on DNA-coated colloids: valency without patches," Phys Rev Lett **113**, 128303 (2014).
44. S. Angioletti-Uberti, B. M. Mognetti, and D. Frenkel, "Re-entrant melting as a design principle for DNA-coated colloids," Nat Mater **11**, 518-522 (2012).
45. H. Tong, P. Tan, and N. Xu, "From Crystals to Disordered Crystals: A Hidden Order-Disorder Transition," Scientific reports **5**, (2015).

46. M. T. U. Casey, "Diffusionless transformations in DNA-mediated alloys of nano-colloids," Ph.D. Thesis, University of Pennsylvania, (2011).
47. R. Dreyfus, M. E. Leunissen, R. Sha, A. V. Tkachenko, N. C. Seeman, D. J. Pine, and P. M. Chaikin, "Simple quantitative model for the reversible association of DNA coated colloids," Phys Rev Lett **102**, 048301 (2009).
48. E. Xi, R. C. Remsing, and A. J. Patel, "Sparse Sampling of Water Density Fluctuations in Interfacial Environments," Journal of chemical theory and computation, (2016).
49. S. Auer and D. Frenkel, "Numerical simulation of crystal nucleation in colloids," Advanced Computer Simulation Approaches for Soft Matter Sciences I **173**, 149-208 (2005).
50. D. Frenkel and B. Smit (2002) *Understanding Molecular Simulation* (Academic Press, New York).
51. K. Kikuchi, M. Yoshida, T. Maekawa, and H. Watanabe, "Metropolis Monte Carlo method as a numerical technique to solve the Fokker—Planck equation," Chemical Physics Letters **185**, 335-338 (1991).
52. T. D. Iracki, D. J. Beltran-Villegas, S. L. Eichmann, and M. A. Bevan, "Charged micelle depletion attraction and interfacial colloidal phase behavior," Langmuir **26**, 18710-18717 (2010).
53. J. Bibette, D. Roux, and F. Nallet, "Depletion interactions and fluid-solid equilibrium in emulsions," Phys Rev Lett **65**, 2470 (1990).
54. J. Savage and A. Dinsmore, "Experimental evidence for two-step nucleation in colloidal crystallization," Phys Rev Lett **102**, 198302 (2009).
55. J. R. Savage, D. W. Blair, A. J. Levine, R. A. Guyer, and A. D. Dinsmore, "Imaging the sublimation dynamics of colloidal crystallites," Science **314**, 795 (2006).